

# Magnetization distribution and orbital moment in the non-Superconducting Chalcogenide Compound $K_{0.8}Fe_{1.6}Se_2$

S. Nandi,<sup>1,2,\*</sup> Y. Xiao,<sup>1</sup> Y. Su,<sup>2</sup> L. C. Chapon,<sup>3</sup> T. Chatterji,<sup>3</sup> W. T. Jin,<sup>1,2</sup> S. Price,<sup>1</sup> T. Wolf,<sup>4</sup> P. J. Brown,<sup>5,3</sup> and Th. Brückel<sup>1,2</sup>

<sup>1</sup>Jülich Centre for Neutron Science JCNS and Peter Grünberg Institut PGI, JARA-FIT, Forschungszentrum Jülich GmbH, D-52425 Jülich, Germany

<sup>2</sup>Jülich Centre for Neutron Science JCNS, Forschungszentrum Jülich GmbH, Outstation at MLZ, Lichtenbergstraße 1, D-85747 Garching, Germany

<sup>3</sup>Institut Laue-Langevin, BP 156, 38042 Grenoble Cedex 9, France

<sup>4</sup>Institut für Festkörperphysik, Karlsruhe Institute of Technology, D-76021 Karlsruhe, Germany

<sup>5</sup>12 Little St. Mary's Lane, Cambridge, CB2 1RR, UK

We have used polarized and unpolarized neutron diffraction to determine the spatial distribution of the magnetization density induced by a magnetic field of 9 T in the tetragonal phase of  $K_{0.8}Fe_{1.6}Se_2$ . The maximum entropy reconstruction shows clearly that most of the magnetization is confined to the region around the iron atoms whereas there is no significant magnetization associated with either Se or K atoms. The distribution of magnetization around the Fe atom is slightly nonspherical with a shape which is extended along the  $\langle 001 \rangle$  direction in the projection. Multipolar refinement results show that the electrons which give rise to the paramagnetic susceptibility are confined to the Fe atoms and their distribution suggests that they occupy  $3d$   $t_{2g}$ -type orbitals with around 66% in those of  $xz/yz$  symmetry. Detail modeling of the magnetic form factor indicates the presence of an orbital moment to the total paramagnetic moment of  $Fe^{2+}$ .

PACS numbers: 75.25.-j, 74.70.Xa, 61.05.F-

## I. INTRODUCTION

The discovery of iron-based superconductors [1] a few years ago has stimulated tremendous research interests worldwide in unconventional high- $T_C$  superconductivity. The new excitement in this field has been generated very recently due to the discovery of the new superconducting compound  $K_xFe_{2-y}Se_2$  with superconducting transition temperature,  $T_C$ , above 30 K [2]. Isostructural  $A_xFe_{2-y}Se_2$  compounds ( $A = Rb, Cs, \text{ and } Tl$  [3–5]) with similar  $T_C$  have been found soon after. One of the fascinating properties of the  $K_xFe_{2-y}Se_2$  superconductors, in contrast to the previously discovered pnictide or chalcogenide superconductors, is the absence of the hole Fermi surface at the Brillouin zone center or the presence of electronic Fermi surface at the zone center [3, 6–8]. This poses a serious challenge to the well accepted theories of the prevailing  $s^\pm$  pairing symmetry driven by the interband scattering as suggested in many weak coupling theories [9]. Another unusual feature of the  $K_xFe_{2-y}Se_2$  superconductors is the presence of an antiferromagnetic order with a large moment ( $\sim 3.3 \mu_B$ ) and very high transition temperature ( $\sim 600$  K) [10] which is in contrast to the parent compound of the pnictide superconductors where Fe moments order antiferromagnetically at considerably lower temperature ( $\sim 150$  K) and with the small ordered magnetic moment ( $\sim 0.5\text{--}0.8 \mu_B$ ) [11, 12]. Initially it was suggested that the superconductivity and antiferromagnetism coexist and compete within the same phase of the  $K_xFe_{2-y}Se_2$  [10]. However, subsequent detailed investigations concluded a phase separation between the vacancy ordered antiferromagnetic phase and a superconducting phase. Based on the observation of the  $\sqrt{5} \times \sqrt{5}$  superlattice in the vacancy ordered antiferromagnetic phase, optimal composition of  $A_2Fe_4Se_5$  has been suggested for the parent

phase [10, 13]. The nature of the superconducting phase is still not settled yet. Both a vacancy free phase with composition  $KFe_2Se_2$  [14–17] and a phase  $A_2Fe_7Se_8$  [17] with Fe vacancies have been found and was assigned to the superconducting phase.

Orbital composition of Fermi surface is very important regarding the pairing mechanism and pairing strength for the Fe-based superconductors. It has been shown theoretically that the strong interorbital interaction is very efficient to achieve superconductivity due to magnetic fluctuations in iron pnictides owing to the distinct orbital character of the Fermi surface [18]. Besides the superconducting properties, physical properties of the Fe-based superconductors are also strongly dependent on the orbital character and occupancies of the Fe  $d$ -orbitals. Indeed, for the superconducting  $K_xFe_{2-y}Se_2$  ( $x \sim 0.76, y \sim 0.22$ ) compounds, a crossover from a low temperature metallic state to an orbital selective Mott phase at high temperature has been observed using Angle-Resolved Photoemission Spectroscopy (ARPES) measurements [19]. ARPES measurements clearly show that the spectral weight of the Fe  $d_{xy}$  orbital near the Fermi surface is diminished at high temperature while the  $d_{xz}/d_{yz}$  orbitals remain metallic. In order to obtain direct information about the electronic states near the Fermi surface we have undertaken magnetization distribution study of the non-superconducting compound  $K_{0.8}Fe_{1.6}Se_2$  using polarized neutron diffraction.

## II. EXPERIMENTAL DETAILS

A good quality single crystal with approximate mass of 300 mg was grown by the Bridgman method [20]. The structural parameters were determined from unpolarized neutron diffraction measurement using the four-circle diffractometer

D9 equipped with a Cu (2 2 0) monochromator to produce a monochromatic neutron beam of 0.838 Å. The flipping ratios were measured using the polarized neutron diffractometer D3 with neutron wavelength of 0.825 Å obtained with a Heusler alloy monochromator with polarization of the incident neutron beam  $P_0 = 0.907(5)$ . Both these instruments are installed on the hot neutron source of the high-flux reactor of the Institute Laue-Langevin in Grenoble. The sample was held at constant temperature in a closed-cycle refrigerator on D9 whereas on D3 it was oriented with a  $\langle 1 1 0 \rangle$  axis parallel to the vertical field direction of a 9 T cryomagnet. The crystallographic notations used here and in the rest of the paper are according to the high temperature tetragonal phase with the  $I4/mmm$  symmetry. The flipping ratios from the  $K_{0.8}Fe_{1.6}Se_2$  crystal were measured in the paramagnetic tetragonal phase at  $T = 600$  K. In a flipping ratio measurement, one measures the ratio  $R = \frac{I^+}{I^-}$ , where  $I^+$  and  $I^-$  are the scattered neutron intensities with neutron polarizations parallel and antiparallel to the applied magnetic field directions, respectively. Because the induced moment is small in  $K_{0.8}Fe_{1.6}Se_2$ , in the limit  $(\gamma r_0/2\mu_B)F_M(\mathbf{Q})/F_N(\mathbf{Q}) \ll 1$ , the flipping ratio,  $R$ , can be expressed as [21]

$$R \approx 1 - \frac{2\gamma r_0 F_M(\mathbf{Q})}{\mu_B F_N(\mathbf{Q})} \quad (1)$$

where,  $\gamma r_0 = 5.36 \times 10^{-15}$  m and  $\mu_B$  is the Bohr magneton.  $F_M(\mathbf{Q})$  and  $F_N(\mathbf{Q})$  are the nuclear and the magnetic structure factors at the reciprocal lattice vector  $\mathbf{Q}$ . Since,  $F_N(\mathbf{Q})$  and  $R$  are known from the unpolarized and polarized neutron diffractions, respectively,  $F_M(\mathbf{Q})$  can be calculated.

### III. EXPERIMENTAL RESULTS

#### A. Macroscopic Characterizations

Figure 1 (a) shows magnetic susceptibility of a single crystal of  $K_{0.8}Fe_{1.6}Se_2$  measured using a Quantum Design vibrating sample magnetometer (VSM). For the magnetization measurements a sample from the same batch as the diffraction measurements was used. Magnetic susceptibility shows a clear kink at  $572 \pm 2$  K, indicating a phase transition from the high temperature vacancy disordered phase to the low temperature vacancy ordered phase. Inset to the Fig. 1 (a) shows  $M$ - $H$  curve measured at  $T = 600$  K. The linear behavior of the  $M$ - $H$  curve confirms the paramagnetic nature of the sample at this temperature. The magnetization induced by a field of 9 T applied along the  $\langle 1 1 0 \rangle$  direction at 600 K was measured as  $0.101(2) \mu_B/\text{f.u.}$  [41] after subtracting very small ferromagnetic contribution of  $0.003(2) \mu_B/\text{f.u.}$  due to impurities (probably pure Fe) [22]. It is the sum of a paramagnetic part due to magnetic excitation of electrons near the Fermi surface and a diamagnetic part to which all electrons contribute. The diamagnetic volume susceptibility is given by the Langevin

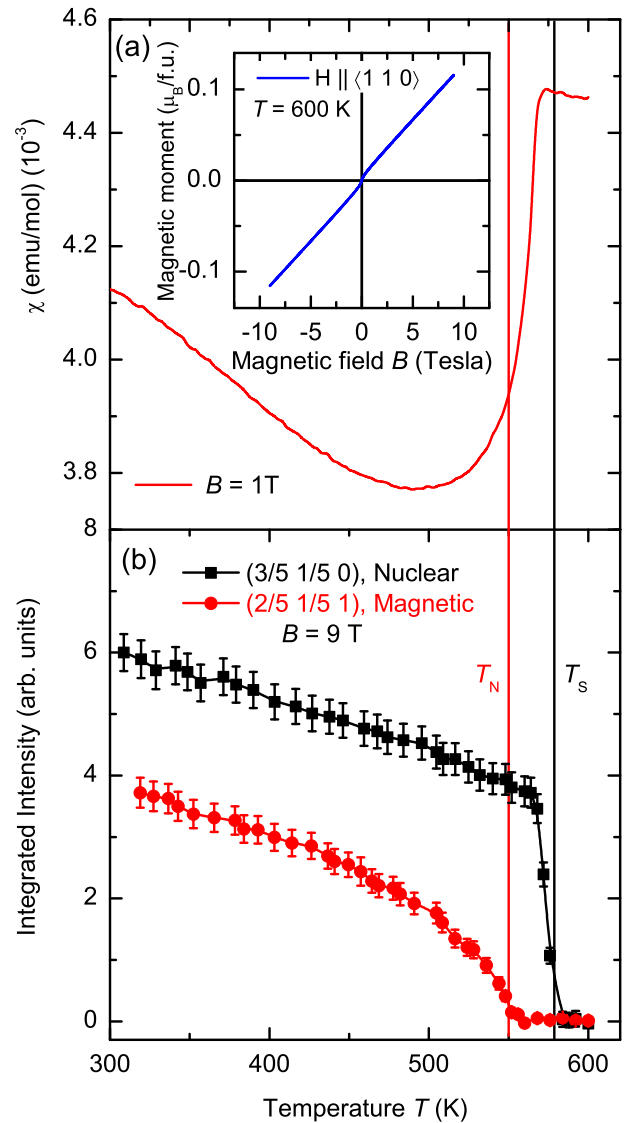


Figure 1: (a) (Color online) Temperature dependence of the magnetic susceptibility measured on heating of the sample in a field of 1 T. Inset shows  $M$ - $H$  curve for the same sample at  $T = 600$  K, above the magnetic ordering transition temperature of Fe. (b) Temperature dependence of the nuclear  $(\frac{3}{5} \frac{1}{5} 0)$  and magnetic  $(\frac{2}{5} \frac{1}{5} 1)$  reflections, signaling the onset of structural and magnetic phase transitions at  $T = 580$  and  $553$  K, respectively.

equation,

$$\chi_{dia} = -\frac{e^2}{6Vmc^2} \sum_i Z_i \langle r^2 \rangle_i \quad (2)$$

The sum is over all the atoms in the unit cell of volume  $V$ ,  $\langle r^2 \rangle_i$  is the mean-square radius of the  $i^{th}$  atom's electron wave function, and  $Z_i$  denotes atomic number. The diamagnetic contribution to the magnetization calculated using Eq. 2 equals to  $-0.014 \mu_B/\text{f.u.}$ , the paramagnetic part of the magnetization therefore equals to  $0.101(2) - (-0.014) = 0.115(2) \mu_B/\text{f.u.}$  which is indicated by the diamond symbol in Fig. 2 [42].

## B. Unpolarized neutron diffraction

In order to characterize the structural and magnetic phase transitions, we have measured the temperature dependence of the nuclear  $(\frac{3}{5} \frac{1}{5} 0)$  and magnetic  $(\frac{2}{5} \frac{1}{5} 1)$  superstructure peaks at a vertical magnetic field of 9 T oriented along the  $\langle 110 \rangle$  direction as shown in Fig. 1 (b). The rapid increase of the intensity of the nuclear  $(\frac{3}{5} \frac{1}{5} 0)$  peak below  $T_S = 580(3)$  K indicates the structural phase transition from the high-temperature Fe-vacancy-disordered phase with  $I4/mmm$  symmetry into the low-temperature Fe-vacancy ordered phase with  $I4/m$  symmetry. The transition temperature is broadly consistent with that determined from magnetic susceptibility measurement. The intensity of the magnetic peak  $(\frac{2}{5} \frac{1}{5} 1)$  vanishes above the antiferromagnetic ordering temperature,  $T_N = 553(3)$  K, of the Fe moments. All the measurements for the determination of magnetization distribution were performed at  $T = 600$  K which is well above both the structural and magnetic phase transitions. Sets of experimental structure factors containing 80 independent reflections within  $\sin\theta/\lambda \leq 0.80 \text{ \AA}^{-1}$  were obtained from the integrated intensities measured on D9 after averaging the intensities over equivalent reflections with a weighted  $R_w F^2$  [43] factor of 4%. These data were used in least-squares refinements of the crystal structure using FullProf [23] in which the variable parameters were the  $z$  coordinate of Se, the anisotropic temperature factors for the three sites, a single extinction parameter  $g$  representing the mosaic spread of the crystal and the site occupancies of the K and Se. The results are summarized in Table I. The small value obtained for  $g$ , which is less than its estimated error, shows that any extinction, if present, is very small. The results are consistent with the neutron powder diffraction results of Bao *et al.* on a similar chemical composition [10].

## C. Polarized neutron diffraction studies

The flipping ratios were measured at an applied magnetic field of 9 T at 600 K at D3. Since the susceptibility of  $K_{0.8}Fe_{1.6}Se_2$  is small ( $\sim 0.1 \mu_B/\text{f.u.}$ ) all the flipping ratios  $R$  are close to unity. Therefore, every reflection was measured for more than one hour to have reasonable counting statistics. The flipping ratios measured for equivalent reflections and for repeated measurements of the same reflection were averaged together to give a mean value of  $R$ , which was used to calculate the magnetic structure factors  $F_M(\mathbf{Q})$  using Cambridge Crystallographic Subroutine Library (CCSL) [26]. Both the observed flipping ratios and the calculated  $F_M(\mathbf{Q})$  are listed in Table II. The nuclear structure factor,  $F_N(\mathbf{Q})$ , was calculated using the parameters obtained from the integrated intensity measurements which are given in Table I.

The diamagnetic contribution to the magnetic structure factor in an applied magnetic field  $B$  is

$$F_{dia} = \frac{BC}{|\mathbf{Q}|} \sum_i \frac{df_i(Q)}{dQ} \exp(i\mathbf{Q} \cdot \mathbf{r}_i) \quad (3)$$

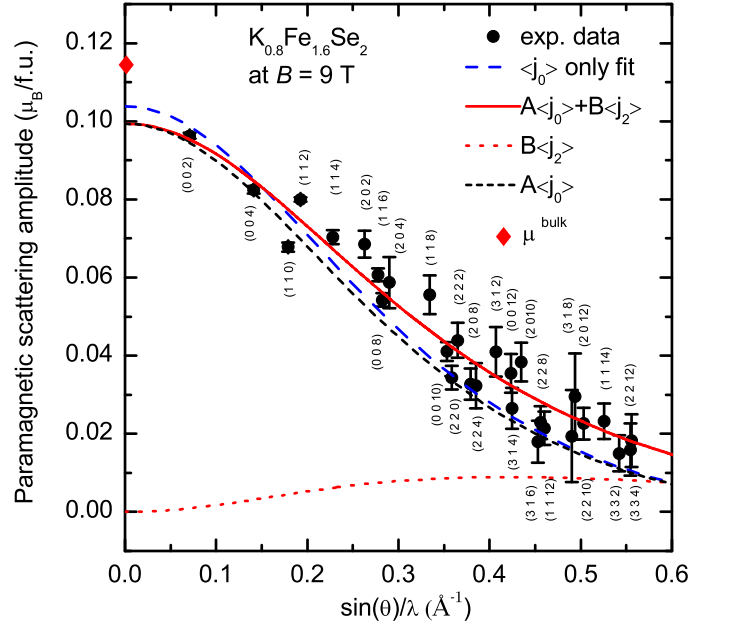


Figure 2: (Color online) Paramagnetic scattering amplitudes of Fe at  $T = 600$  K. The large-dashed curve (blue) shows fitting using the  $\langle j_0 \rangle$  form factor for  $Fe^{2+}$ , Ref. 24. The solid (red) curve shows fitting with  $\langle j_0 \rangle$  and  $\langle j_2 \rangle$  form factors with individual contributions are indicated by short-dashed (black) and dotted (red) lines, respectively [25]. A and B are fitting parameters.

where  $f_i(Q)$  is the atomic form factor of the  $i^{th}$  atom and  $\mathbf{r}_i$  its position in the unit cell [27]. The constant  $C$  has the value  $1.52 \times 10^{-5} \mu_B T^{-1} \text{ \AA}^2$  [28]. The diamagnetic contributions to the magnetic structure factors were calculated using Eq. 3 and are given in Table II. The values  $F_{dia}$  were subtracted from the magnetic structure factors  $F_M$  to obtain the paramagnetic structure factors  $F_{para}$  which are also listed in Table II. The geometric structure factor of Fe atoms for the  $(hkl)$  reflections can be written as:

$$F_{geo} = 2 \cos(\pi l/2) (e^{i\pi h} + e^{i\pi k}) \quad (4)$$

which is either +4 or -4 depending on the values of  $h, k, l$  assuming full occupancy of the Fe site. In Fig. 2, we show the effective paramagnetic scattering amplitude, obtained by dividing each  $F_{para}$  by  $F_{geo} \times T(hkl)$  and multiplied by the number of Fe atoms in the unit cell. It can be seen that most of the paramagnetic scattering amplitude lies reasonably close to theoretical spherical form factor  $\langle j_0 \rangle$  of  $Fe^{2+}$  [25]. This result signifies that most of the paramagnetic scattering amplitude is associated with the  $Fe^{2+}$  moments.

To have a model free reconstruction of magnetization density, we have used maximum entropy method using MEMSYS III subroutine library [29]. This method has been shown to give more reliable results from sparse and noisy data compared to conventional Fourier analysis [30]. We have used this method to clarify the shape of the distribution. Figure 3 shows maximum entropy reconstruction of the magnetization distri-

Table I: Parameters obtained in least-squares refinements of integrated intensities measured at  $T = 600$  K on D9.

Atom	Position in $I4/mmm$			$\beta_{11} = \beta_{22}$	$\beta_{33}$	$\beta_{12}, \beta_{13}, \beta_{23}$	$n$	
	site	$x$	$y$					$z$
K	$2a$	0	0	0	0.13(2)	0.010 (1)	0	0.82(4)
Fe	$4d$	$\frac{1}{2}$	0	$\frac{1}{4}$	0.056(2)	0.0059(3)	0	0.81(1)
Se	$4e$	0	0	0.3532(2)	0.060(3)	0.0052(3)	0	1

Extinction  $g$  ( $\text{rad}^{-1}$ ) =  $2 \pm 2$ ,  $R_{F^2}$ ,  $R_{wF^2}$ ,  $R_F$ ,  $\chi^2$ : 6.8, 7.3, 6.2, 3.0  
 $a = 3.945$  (2) Å,  $c = 14.163$ (4) Å

Definitions: Thermal factor  $T(hkl) = \exp\{-\beta_{11}h^2 + \beta_{22}k^2 + \beta_{33}l^2 + 2\beta_{12}hk + 2\beta_{13}hl + 2\beta_{23}kl\}$

$$R_{F^2} = 100 \frac{\sum_n |G_{obs,n}^2 - \sum_k G_{calc,k}^2|}{\sum_n G_{obs,n}^2}, R_{wF^2} = 100 \sqrt{\frac{\sum_n w_n (G_{obs,n}^2 - \sum_k G_{calc,k}^2)^2}{\sum_n w_n G_{obs,n}^4}}, R_F = 100 \frac{\sum_n |G_{obs,n} - \sqrt{\sum_k G_{calc,k}^2}|}{\sum_n G_{obs,n}}$$

Where the index  $n$  runs over the observations and the index  $k$  runs over the reflections contributing to the observation  $n$ .

$G^2$  is the square of the structure factor.  $w_n = 1/\sigma_n^2$ , is the weight where  $\sigma_n^2$  is the variance of  $G_{obs,n}$ .

Table II: Observed and calculated magnetic structure factors for the  $\text{K}_{0.8}\text{Fe}_{1.6}\text{Se}_2$  at 600 K and at  $B = 9$  T.

$h$	$k$	$l$	$\sin\theta/\lambda$ Å <sup>-1</sup>	(1-R) × 10 <sup>3</sup>	$F_M$ m $\mu_B$ /f.u.	$F_{dia}$ m $\mu_B$ /f.u.	$F_{para}$ m $\mu_B$ /f.u.	$F_{calc}^a$ m $\mu_B$ /f.u.
0	0	2	0.0706	26.8 ± 0.3	-92.9 ± 1.2	1.13	-94.0 ± 1.2	-94.0
0	0	4	0.1412	97.9 ± 2.2	74.9 ± 1.6	-0.02	74.9 ± 1.6	77.0
1	1	0	0.1791	-101.8 ± 2.9	-61.1 ± 1.8	-0.46	-60.6 ± 1.8	-69.0
1	1	2	0.1925	28.6 ± 0.5	69.3 ± 1.1	-0.42	69.8 ± 1.1	66.0
1	1	4	0.2281	12.5 ± 0.6	-56.6 ± 2.6	0.61	-57.2 ± 2.6	-55.0
2	0	2	0.2630	10.3 ± 0.9	-53.1 ± 4.4	0.27	-53.4 ± 4.4	-45.0
1	1	6	0.2774	9.8 ± 0.5	43.2 ± 2.4	-0.53	43.8 ± 2.4	42.0
0	0	8	0.2824	10.2 ± 0.6	36.6 ± 2.3	-0.43	37.4 ± 2.3	37.0
2	0	4	0.2900	47.5 ± 7.8	42.6 ± 7.7	-0.04	42.6 ± 7.7	39.0
1	1	8	0.3345	49.4 ± 7.8	-33.9 ± 5.2	0.03	-33.9 ± 5.2	-29.0
0	0	10	0.3531	6.5 ± 0.8	-22.3 ± 2.6	0.28	-22.6 ± 2.6	-22.0
2	2	0	0.3583	5.0 ± 0.8	21.6 ± 3.3	-0.32	21.9 ± 3.3	27.0
2	2	2	0.3651	12.0 ± 2.1	-27.2 ± 4.7	0.14	-27.3 ± 4.7	-26.0
2	0	8	0.3794	5.0 ± 1.1	17.6 ± 3.7	-0.20	17.8 ± 3.7	22.0
2	2	4	0.3851	45.9 ± 13.6	18.7 ± 5.4	-0.01	18.7 ± 5.4	23.0
3	1	2	0.4067	12.8 ± 3.3	22.7 ± 5.9	-0.07	22.8 ± 5.9	18.0
0	0	12	0.4237	9.6 ± 2.3	14.9 ± 3.7	-0.10	15.0 ± 3.7	11.0
3	1	4	0.4247	3.9 ± 1.3	-13.6 ± 4.4	0.16	-13.8 ± 4.4	-16.0
2	0	10	0.4345	5.1 ± 1.2	-16.7 ± 3.8	0.16	-16.9 ± 3.8	-14.0
3	1	6	0.4531	2.6 ± 1.3	8.1 ± 4.0	-0.13	8.2 ± 4.0	14.0
2	2	8	0.4562	4.6 ± 1.5	9.9 ± 3.1	-0.11	10.0 ± 3.1	14.0
1	1	12	0.4600	8.1 ± 2.8	-8.0 ± 2.8	0.05	-8.1 ± 2.8	-13.0
3	1	8	0.4901	12.5 ± 21.7	-7.5 ± 13.0	0.01	-7.5 ± 13.0	-10.0
2	0	12	0.4936	7.0 ± 6.5	9.9 ± 8.6	-0.05	10.0 ± 8.6	8.0
2	2	10	0.5030	3.6 ± 1.1	-7.8 ± 2.5	0.10	-7.9 ± 2.5	-10.0
1	1	14	0.5257	3.3 ± 1.2	6.3 ± 2.2	-0.08	6.4 ± 2.2	5.0
3	3	2	0.5420	6.0 ± 3.1	5.3 ± 2.7	-0.02	5.3 ± 2.7	8.0
2	2	12	0.5548	4.5 ± 3.1	4.3 ± 2.9	-0.03	4.3 ± 2.9	6.0
3	3	4	0.5556	3.2 ± 1.9	-6.0 ± 3.6	0.06	-6.0 ± 3.6	-7.0

<sup>a</sup>using a constrained multipole model with an orbital moment.

bution projected down to the  $[1\ 1\ 0]$  plane using the measured magnetic structure factors for the  $[H\ H\ L]$  type of reflections. The reconstruction shows clearly that the majority of magnetization is confined to the region around the iron atoms. However, a very small magnetization ( $\leq 0.01\ \mu_B\text{Å}^{-2}$ ) can be seen around the Se atoms signifying a possible hybridization between the Fe and Se. The magnetization around the Fe atom

is slightly nonspherical with a shape that appears to extend in the  $\langle 001 \rangle$  direction of the projection.

Further analysis of the measured paramagnetic scattering amplitude was obtained by fitting the magnetic structure factors to a multipole model in which they are expressed as

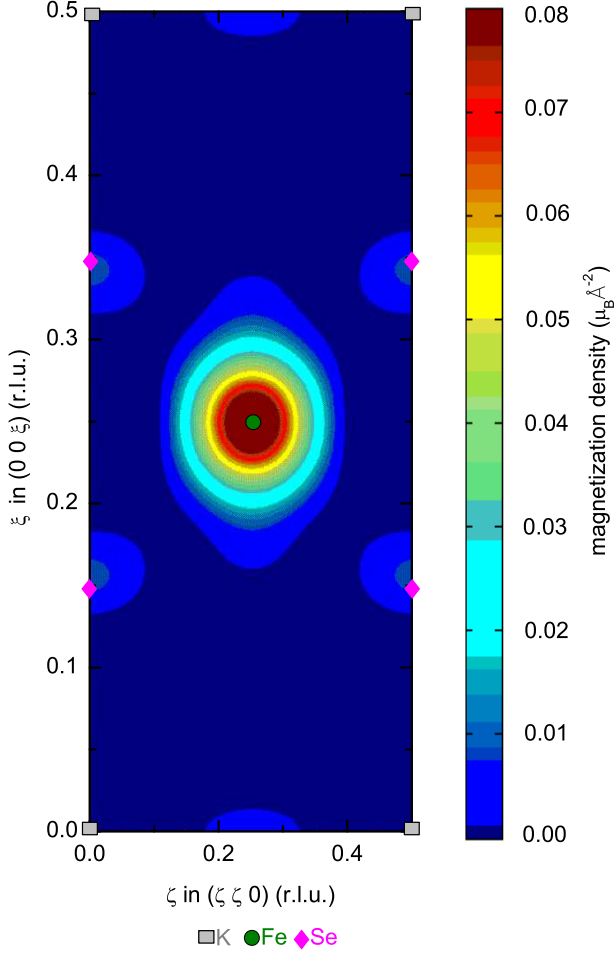


Figure 3: (Color online) Maximum-entropy reconstruction of the magnetization distribution in tetragonal  $\text{K}_{0.8}\text{Fe}_{1.6}\text{Se}_2$  at 600 K projected down to  $[1\ 1\ 0]$ .

$$F_M(\mathbf{Q}) = a_0 \langle j_0 | \mathbf{Q} \rangle Y(00) + \mu_L \langle j_2 | \mathbf{Q} \rangle + \sum_{l=2,4} \langle j_l | \mathbf{Q} \rangle \sum_{m=-l}^{m=l} a_{lm} Y_{\hat{Q}}(lm\pm) \quad (5)$$

where,  $a_0 = \mu_s + \mu_l$  is the total magnetic moment of Fe.  $\mu_s$  and  $\mu_l$  are the spin and orbital contributions respectively.  $\langle j_l | \mathbf{Q} \rangle$  are the form factor for a  $\text{Fe}^{2+}$  and  $Y_{\hat{Q}}(lm\pm)$  are the real combinations of spherical harmonic functions written as,

$$Y_{\hat{Q}}(lm\pm) = \frac{1}{\sqrt{2}} [Y_l^{-m}(\hat{Q}) \pm (-1)^m Y_l^m(\hat{Q})] \quad (6)$$

The point group symmetry of Fe site,  $\bar{4}m2$ , limits the nonzero coefficients  $a_{lm}$  to  $a_{20}$ ,  $a_{40}$  and  $a_{44}$ . Different models have been considered for fitting the paramagnetic scattering amplitude in Fig. 2, namely, (a) a dipole model with only first two terms in the Eq. 5, and (b) a multipole model when all the terms in the Eq. 5 are retained. Both the dipole and

Table III: Fitting results of the measured form factors with different models as described in the text and the corresponding agreement factors.

Model	$(\mu_s + \mu_l) \langle j_0 \rangle$ in $\mu_B/\text{Fe}$	$\mu_l \langle j_2 \rangle$ in $\mu_B/\text{Fe}$	$\chi^2$	$R_w$
dipole	0.0320(5)	0	3.3	12.6%
multipole <sup>a</sup>	0.0306(4)	0.014(4)	2.0	7.9%
	0.0319(4)	0	3.4	12.5%
	0.0306(4)	0.014(4)	2.2	7.7%

$R_w = 100 \frac{\sum_n w_n |F_{obs,n}^2 - F_{calc,n}^2|}{\sum_n w_n F_{obs,n}^2}$ .  $w_n = 1/\sigma_n^2$ , is the weight where  $\sigma_n^2$  is the variance of  $F_{obs,n}$

<sup>a</sup>Multipole parameters constrained to give only  $t_{2g}$  type orbitals.

multipole models have been considered with and without the orbital moment. The results of different fitting models have been summarized in Table III. It can be easily seen that the inclusion of orbital part increases the quality of fit in both the low and high  $\mathbf{Q}$  regions of the form factor and the agreement factors significantly. The obtained ratio of  $\frac{\mu_l}{\mu_s} \approx 0.88$  signifies dominant contribution of the orbital moment to the total paramagnetic scattering amplitude of  $\text{Fe}^{2+}$ .

In a site with fourfold symmetry the  $d$  orbitals split into the singlet states:  $d_{3z^2-r^2}$ ,  $d_{x^2-y^2}$ , and  $d_{xy}$  and a doublet combination of  $d_{xz}$  and  $d_{yz}$ . The first two singlet states are derived from the cubic  $e_g$  functions and the third singlet and the doublet from the  $t_{2g}$  ones. The occupancies of these four nondegenerate orbitals can be derived directly from the coefficients  $a_{lm}$  [31]. However, the parameters obtained from the unconstrained fit lead to unphysical, negative occupancies for the  $d_{xy}$  orbital with large estimated standard deviations for all the orbitals as can be seen from Table IV. Band structure calculations as well as photoemission spectroscopy measurements indicate that the  $t_{2g}$  orbitals dominate at the Fermi surface [6, 7, 19, 32]. Therefore, a constrained fit [31] in which the ratio between the  $a_{lm}$  was fixed to correspond to occupancy of the  $t_{2g}$ -type orbitals only, gave equally good agreement factor as well as less standard deviation of the fitted parameters as shown in Table IV. The refinement shows that  $\sim 66\%$  of the electrons occupy doubly degenerate  $d_{xz}/d_{yz}$  orbitals and  $\sim 34\%$  of those are in the  $d_{xy}$  orbital. The magnetic structure factors calculated for this constrained multipole model are given together with the measured values and the diamagnetic corrections in Table II.

There have been a few reports of magnetization distribution for the superconducting and non superconducting Fe based compounds [21, 31, 33–35]. Of particular interest are the results of  $\text{BaFe}_2\text{As}_2$  by Brown *et al.* [31] who have shown that most of the magnetization is associated with the Fe atoms and the distribution is non-spherical with an extension along the  $\langle 111 \rangle$  direction. For the superconducting  $\text{Ba}(\text{Fe}_{1-x}\text{Co}_x)_2\text{As}_2$  samples both Prokeš *et al.* [33] and Lester *et al.* [21] have concluded that the magnetization is rather extended along the  $\langle 110 \rangle$  direction. The change in dis-

tribution between the doped and undoped samples is due to the doping induced modifications of the relevant bands near the Fermi surface as suggested by Lester *et al.* [21]. In contrast to all of the investigated Fe-pnictides,  $K_{0.8}Fe_{1.6}Se_2$  shows distribution elongated along the  $\langle 001 \rangle$  direction. The results of the present experiment show that at least 96% of the electrons in  $K_{0.8}Fe_{1.6}Se_2$ , which give rise to the paramagnetic susceptibility, are localized on the Fe atoms with a radial distribution similar to that of a  $Fe^{2+}$ . Their angular distribution shows that they occupy the  $t_{2g}$ -type orbitals with a strong preference for the doubly degenerate  $xz/yz$  type which is in agreement with the slight elongation observed along the  $\langle 001 \rangle$  direction for the maximum entropy map in Fig. 3. For the  $BaFe_2As_2$ , the  $xy$  ( $\sim 52\%$ ) orbitals are more occupied than the  $xz/yz$  ( $\sim 48\%$ ) orbitals which is opposite to the results for the  $K_{0.8}Fe_{1.6}Se_2$  as shown in Table IV. This difference in occupancy for the  $t_{2g}$  orbitals and the corresponding magnetization distribution in different compounds might be due to the subtle interplay between the crystal field effects and Hund's rule coupling [36].

Most surprising result of the present study is the presence of an orbital moment to the total paramagnetic moment of  $K_{0.8}Fe_{1.6}Se_2$ . Previous studies also hinted existence of orbital moment [21, 33]. For the superconducting  $Ba(Fe_{1-x}Co_x)_2As_2$  samples, Lester *et al.* [21] have found that at least  $\frac{2}{3}$  of the normal state susceptibility does not vanish at the lowest achievable temperature of 2 K. They have attributed the remaining susceptibility to the orbital contribution of Van Vleck type or due to the presence of residual quasiparticle density of states at the Fermi surface. Our very accurate form factor measurement allows us to quantify the orbital contribution relative to the spin contribution. The observed form factor of  $Fe^{2+}$  is best fitted using  $\sim 46\%$  orbital and  $\sim 54\%$  spin contributions to the total magnetization. The amount of orbital contribution is unusually high keeping in mind that the orbital moment is generally quenched in a  $3d$ -orbital system due to the crystal field effects. Nevertheless, similarly large orbital contribution has been found for the Vanadium  $d$ -electrons in classical  $s$ -wave superconductor  $V_3Si$  using polarized neutrons [37]. For the Fe-based superconductors, band structure calculations also predicted that the orbital contribution is larger than the spin contribution [38]. Our results provide first experimental hint of non-negligible orbital contribution to the total paramagnetic susceptibility of  $K_{0.8}Fe_{1.6}Se_2$ . Strongly anisotropic and weakly temperature dependent magnetic susceptibility observed in the  $A_xFe_{2-y}Se_2$  ( $A = K, Rb, Cs$ ) systems [39, 40] might be related to the presence of large orbital contribution since the spin contribution is strongly temperature dependent.

#### IV. CONCLUSION

In summary, we have determined magnetization distribution in  $K_{0.8}Fe_{1.6}Se_2$  using polarized neutron diffraction. Magnetic structure factors derived from the polarization dependence of the intensities of the Bragg reflections were used

Table IV: Multipole amplitudes and  $3d$  orbital occupancies determined from the signed magnetic structure factors using CCSL.

Function	coefficient	all $d^a$	Amplitudes (in $\mu_B/Fe$ )	
			$t_{2g}$ only <sup>b</sup>	
Y(00)	$a_0$	0.0306(5)	0.0306(4)	
Y(20)	$a_{20}$	0.04(10)	-0.03(9)	
Y(40)	$a_{40}$	-0.20(40)	-0.39(6)	
Y(44+)	$a_{44}$	0.48(58)	-0.37(7)	
	$\mu_L$	0.017(4)	0.014(4)	
$\chi^2$		2.2	2.2	
Occupancies (%)				
orbital		all $d^a$	$t_{2g}$ only <sup>b</sup>	
$3z^2-r^2$		12(24)	0	
$x^2-y^2$		40(35)	0	
$xy$		-6(35)	34(7)	
$xz, yz$		54(30)	66(7)	

<sup>a</sup>All multipole parameters allowed by the  $\bar{4}m2$  point group symmetry.

<sup>b</sup>Multipole parameters constrained to give only  $t_{2g}$  type orbitals.

to make a maximum-entropy reconstruction of the distribution projected on the  $[110]$  plane. The reconstruction shows clearly that the magnetization is confined to the region around the iron atoms. A very small magnetization around the Se atoms hints towards a possible hybridization between the Fe and Se. The distribution of magnetization around the Fe atom is slightly nonspherical with a shape which is extended in the  $\langle 001 \rangle$  direction in the projection. These results show that the electrons which give rise to the paramagnetic susceptibility are confined to the Fe atoms and their distribution suggests that they occupy  $3d$   $t_{2g}$ -type orbitals with 66% in those of  $xz/yz$  symmetry. Orbital moment contributes significantly to the total paramagnetic moment of Fe and might be responsible for the anisotropic properties of the Fe-based superconductors.

S. N. likes to acknowledge M. Angst for helpful discussions and M. Vial and A. John for technical assistance.

\* Electronic address: [s.nandi@fz-juelich.de](mailto:s.nandi@fz-juelich.de)

- [1] Y. Kamihara, T. Watanabe, M. Hirano, and H. Hosono, *J. Am. Chem. Soc.* **130**, 3296 (2008).
- [2] J. Guo, S. Jin, G. Wang, S. Wang, K. Zhu, T. Zhou, M. He, and X. Chen, *Phys. Rev. B* **82**, 180520 (2010).
- [3] A. F. Wang, J. J. Ying, Y. J. Yan, R. H. Liu, X. G. Luo, Z. Y. Li, X. F. Wang, M. Zhang, G. J. Ye, P. Cheng, et al., *Phys. Rev. B* **83**, 060512 (2011).
- [4] A. Krzton-Maziopa, Z. Shermadini, E. Pomjakushina, V. Pomjakushin, M. Bendele, A. Amato, R. Khasanov, H. Luetkens, and K. Conder, *J. Phys.: Condens. Mat.* **23**, 052203 (2011).
- [5] M.-H. Fang, H.-D. Wang, C.-H. Dong, Z.-J. Li, C.-M. Feng, J. Chen, and H. Q. Yuan, *Europhys. Lett.* **94**, 27009 (2011).
- [6] Y. Zhang, L. X. Yang, M. Xu, Z. R. Ye, F. Chen, C. He, H. C. Xu, J. Jiang, B. P. Xie, J. J. Ying, et al., *Nat. Mater.* **10**, 273

- (2011).
- [7] T. Qian, X.-P. Wang, W.-C. Jin, P. Zhang, P. Richard, G. Xu, X. Dai, Z. Fang, J.-G. Guo, X.-L. Chen, et al., *Phys. Rev. Lett.* **106**, 187001 (2011).
- [8] D. Mou, S. Liu, X. Jia, J. He, Y. Peng, L. Zhao, L. Yu, G. Liu, S. He, X. Dong, et al., *Phys. Rev. Lett.* **106**, 107001 (2011).
- [9] I. I. Mazin and J. Schmalian, *Physica C* **469**, 614 (2009).
- [10] W. Bao, Q. Huang, G. F. Chen, M. A. Green, D. M. Wang, J. B. He, X. Q. Wang, and Y. Qiu, *Chin. Phys. Lett.* **28**, 086104 (2011).
- [11] C. de la Cruz, Q. Huang, J. W. Lynn, J. Li, W. Ratcliff II, J. L. Zarestky, H. A. Mook, G. F. Chen, J. L. Luo, N. L. Wang, et al., *Nature (London)* **453**, 899 (2008).
- [12] D. C. Johnston, *Adv. Phys.* **59**, 803 (2010).
- [13] F. Ye, S. Chi, W. Bao, X. F. Wang, J. J. Ying, X. H. Chen, H. D. Wang, C. H. Dong, and M. Fang, *Phys. Rev. Lett.* **107**, 137003 (2011).
- [14] A. Ricci, N. Poccia, G. Campi, B. Joseph, G. Arrighetti, L. Barba, M. Reynolds, M. Burghammer, H. Takeya, Y. Mizuguchi, et al., *Phys. Rev. B* **84**, 060511 (2011).
- [15] R. H. Yuan, T. Dong, Y. J. Song, P. Zheng, G. F. Chen, J. P. Hu, J. Q. Li, and N. L. Wang, *Sci. Rep.* **2**, 221 (2012).
- [16] W. Li, H. Ding, P. Deng, K. Chang, C. L. Song, K. He, L. L. Wang, X. C. Ma, J. P. Hu, X. Chen, et al., *Nat. Phys.* **8**, 126 (2012).
- [17] X. Ding, D. Fang, Z. Wang, H. Yang, J. Liu, Q. Deng, G. Ma, C. Meng, Y. Hu, and H.-H. Wen, *Nat. Commun.* **4**, 1987 (2013).
- [18] J. Zhang, R. Sknepnek, R. M. Fernandes, and J. Schmalian, *Phys. Rev. B* **79**, 220502 (2009).
- [19] M. Yi, D. H. Lu, R. Yu, S. C. Riggs, J.-H. Chu, B. Lv, Z. K. Liu, M. Lu, Y.-T. Cui, M. Hashimoto, et al., *Phys. Rev. Lett.* **110**, 067003 (2013).
- [20] S. Landsgesell, D. Abou-Ras, T. Wolf, D. Alber, and K. Prokeš, *Phys. Rev. B* **86**, 224502 (2012).
- [21] C. Lester, J.-H. Chu, J. G. Analytis, A. Stunault, I. R. Fisher, and S. M. Hayden, *Phys. Rev. B* **84**, 134514 (2011).
- [22] I. Felner, S. Jin, G. Wang, S. Wang, K. Zhu, and T. Zhou, *J. Supercond. Nov. Magn.* **24**, 2033 (2011).
- [23] J. Rodríguez-Carvajal (2012), program FULLPROF, Version: May-2012, ILL, Grenoble, France.
- [24] A. J. Freeman and R. E. Watson, *Acta Crystallogr.* **14**, 231 (1961).
- [25] P. J. Brown, in *International Tables for Crystallography*, edited by E. Prince (International Union of Crystallography, 2006), vol. C, chap. 4.4, pp. 454–461.
- [26] P. J. Brown and J. Matthewman, in *Cambridge Crystallographic Subroutine Library, Rutherford Appleton Laboratory Report No. RAL93-009*. (1993).
- [27] E. N. Maslen, A. Fox, and M. A. O’Keefe, in *International Tables for Crystallography*, edited by E. Prince (International Union of Crystallography, 2006), vol. C, chap. 6.1, pp. 578–580.
- [28] C. Stassis, *Phys. Rev. Lett.* **24**, 1415 (1970).
- [29] S. F. Gull and J. Skilling, MEMSYS III Quantified Maximum Entropy Subroutine Library, Meldreth, U.K., 1989.
- [30] R. J. Papoular and B. Gillon, *Europhys. Lett.* **13**, 429 (1990).
- [31] P. J. Brown, T. Chatterji, A. Stunault, Y. Su, Y. Xiao, R. Mittal, T. Brückel, T. Wolf, and P. Adelman, *Phys. Rev. B* **82**, 024421 (2010).
- [32] D.-Y. Liu, Y.-M. Quan, Z. Zeng, and L.-J. Zou, *Physica B* **407**, 1139 (2012).
- [33] K. Prokeš, A. Gukasov, D. N. Argyriou, S. L. Bud’ko, P. C. Canfield, A. Kreyssig, and A. I. Goldman, *Europhys. Lett.* **93**, 32001 (2011).
- [34] W. Ratcliff, P. A. Kienzle, J. W. Lynn, S. Li, P. Dai, G. F. Chen, and N. L. Wang, *Phys. Rev. B* **81**, 140502 (2010).
- [35] Y. Lee, D. Vaknin, H. Li, W. Tian, J. L. Zarestky, N. Ni, S. L. Bud’ko, P. C. Canfield, R. J. McQueeney, and B. N. Harmon, *Phys. Rev. B* **81**, 060406 (2010).
- [36] Z. P. Yin, K. Haule, and G. Kotliar, *Nat. Mater.* **10**, 932 (2011).
- [37] C. G. Shull and F. A. Wedgwood, *Phys. Rev. Lett.* **16**, 513 (1966).
- [38] Y. Su and T. Li, arXiv:1103.1056v2 (unpublished).
- [39] H. Lei and C. Petrovic, *Phys. Rev. B* **83**, 184504 (2011).
- [40] R. H. Liu, X. G. Luo, M. Zhang, A. F. Wang, J. J. Ying, X. F. Wang, Y. J. Yan, Z. J. Xiang, P. Cheng, G. J. Ye, et al., *Europhys. Lett.* **94**, 27008 (2011).
- [41] In this paper, we have used one formula unit as one crystallographic unit cell. Therefore, in one formula unit, on the average there are 3.6 Fe atoms considering the Fe vacancies in the high temperature phase.
- [42] The obtained value is slightly larger than the interpolated  $\mathbf{Q}(0)$  value of the magnetic form factor. This difference might be due to the presence of large diffuse scattering at  $T = 600$  K or might be due to over-estimation of the diamagnetic contribution since it is apparently calculated for free atoms. Therefore, we have not included the  $\mathbf{Q}(0)$  value for the form factor refinement and maximum entropy calculation.
- [43] The weighted  $R$  factor for the equivalent reflections is defined as :  $R_{wF^2} = 100 \left[ \frac{\sum_n w_n (I_{obs,n} - I_{mean})^2}{\sum_n w_n I_{mean}^2} \right]^{1/2}$ .  $w_n = 1/\sigma_n^2$ , is the weight where  $\sigma_n^2$  is the variance of  $I$ .